Report

Cell Reports

In Vivo Formation of Vacuolated Multi-phase Compartments Lacking Membranes

Graphical Abstract

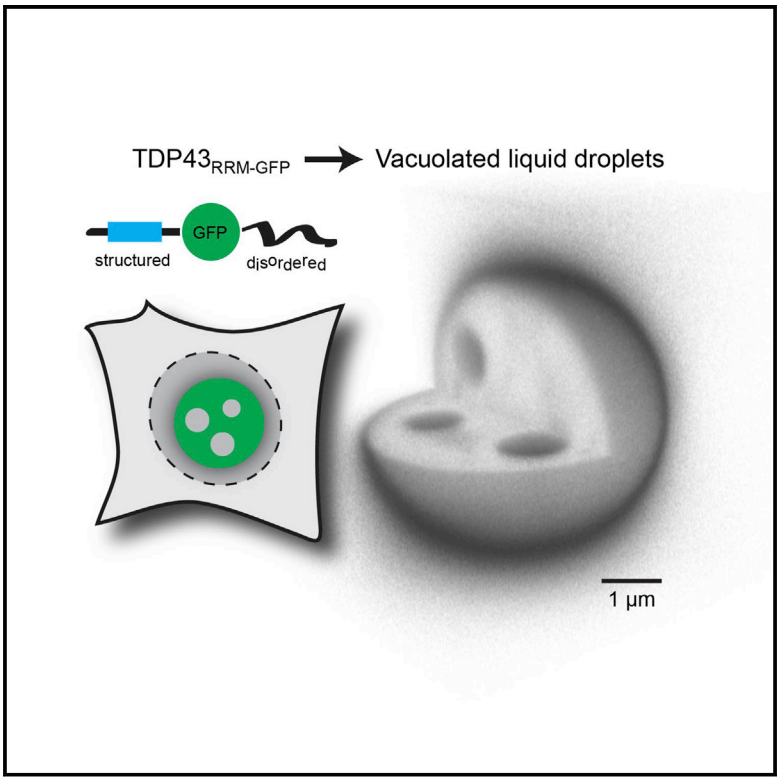

Highlights

- The N and C termini of TDP43 can drive the formation of giant liquid droplets in cells
- Droplets contain nucleoplasm-filled vacuoles despite lacking membranes
- ALS-causative point mutants in the C terminus alter phase properties
- Nearly identical TDP43 variants assemble into coexisting, yet largely immiscible phases

Authors

Hermann Broder Schmidt, Rajat Rohatgi

Correspondence

shb@stanford.edu (H.B.S.),
rrohatgi@stanford.edu (R.R.)

In Brief

Membrane-less organelles generated through liquid-liquid phase separation play important roles in sub-cellular organization. Schmidt and Rohatgi find that an intrinsically disordered protein domain can nucleate the assembly of multi-phase liquid droplets with dynamic, vesicle-like internal vacuoles that approach the morphological complexity of membrane-bound structures like multi-vesicular bodies.

Schmidt & Rohatgi, 2016, Cell Reports *16*, 1228–1236
August 2, 2016
http://dx.doi.org/10.1016/j.celrep.2016.06.088

OPEN ACCESS
CellPress

Cell Reports
Report

In Vivo Formation of Vacuolated Multi-phase Compartments Lacking Membranes

Hermann Broder Schmidt[1,*] and Rajat Rohatgi[1,2,*]
[1]Department of Biochemistry, Stanford University School of Medicine, Stanford, CA 94305, USA
[2]Department of Medicine, Stanford University School of Medicine, Stanford, CA 94305, USA
*Correspondence: shb@stanford.edu (H.B.S.), rrohatgi@stanford.edu (R.R.)
http://dx.doi.org/10.1016/j.celrep.2016.06.088

SUMMARY

Eukaryotic cells contain membrane-less organelles, including nucleoli and stress granules, that behave like liquid droplets. Such endogenous condensates often have internal substructure, but how this is established in the absence of membrane encapsulation remains unclear. We find that the N- and C-terminal domains of TDP43, a heterogeneous nuclear ribonucleoprotein implicated in neurodegenerative diseases, are capable of driving the formation of sub-structured liquid droplets in vivo. These droplets contain dynamic internal "bubbles" of nucleoplasm, reminiscent of membrane-based multi-vesicular endosomes. A conserved sequence embedded within the intrinsically disordered region (IDR) of TDP43 promotes the formation of these multi-phase assemblies. Disease-causing point mutations in the IDR can change the propensity to form bubbles, protein dynamics within the phase, or phase-environment exchange rates. Our results show that a single IDR-containing protein can nucleate the assembly of compartmentalized liquid droplets approximating the morphological complexity of membrane-bound organelles.

INTRODUCTION

Subcellular compartmentalization, a defining feature of eukaryotic cells, is established by membrane-enclosed organelles as well as by "membrane-less" assemblies generated by the condensation of protein and nucleic acid components into liquid phases that self-segregate from the bulk aqueous phase of the cell. Examples of structures generated by such liquid-liquid de-mixing include nucleoli, processing bodies, and stress granules (Mitrea and Kriwacki, 2016). Their liquid-like composition and lack of membranes allows these structures to remain in a dynamic equilibrium with their surrounding and rapidly rearrange in response to intra- or extracellular cues (Wang et al., 2014; Wippich et al., 2013). Despite this fluid nature, membrane-less organelles (MLOs) can contain morphologically, physically, and functionally distinct regions. How such defined regions remain segregated in the context of an overall fluid nature is poorly understood (Bergeron-Sandoval et al., 2016).

MLOs often include proteins containing intrinsically disordered regions (IDRs) that resemble aggregation-prone prion domains (Malinovska et al., 2013; Toretsky and Wright, 2014). In vitro and in vivo studies of IDR-containing heterogeneous nuclear ribonucleoproteins (hnRNPs), including FUS, hnRNPA1, and hnRNPA2, illustrated the ability of IDRs to drive liquid-liquid phase separation (Burke et al., 2015; Lin et al., 2015; Molliex et al., 2015; Patel et al., 2015). However, many IDR-containing proteins are not only integral components of MLOs, but also form aggregates in neurodegenerative diseases. Indeed, it was recently demonstrated that the amyotrophic lateral sclerosis (ALS)- and frontotemporal dementia (FTD)-linked proteins FUS and hnRNPA1 undergo a liquid-to-solid transition upon aging in vitro and suggested that this transformation may be important in neurodegeneration (Li et al., 2013; Lin et al., 2015; Molliex et al., 2015; Patel et al., 2015). TDP43, another hnRNP family member with described functions in transcriptional regulation and splicing (Buratti and Baralle, 2008), is present in ~95% and ~45% of all aggregates in patients with ALS and FTD, respectively. These TDP43 aggregates may be mechanistically linked to neurodegeneration since mutations in *TARDBP*, the gene encoding TDP43, can cause ALS and ALS-FTD (Kabashi et al., 2008; Sreedharan et al., 2008). Intriguingly, a recent in vitro study showed that TDP43 can autonomously phase-separate (Molliex et al., 2015). Motivated by these findings and the known association of TDP43 with MLOs such as stress and transport granules (Alami et al., 2014; Colombrita et al., 2009; McDonald et al., 2011), we explored the hypothesis that TDP43 may form liquid-like phases in cells and that ALS-linked mutations can alter the phase properties. We find that TDP43 has the potential to form micron-sized liquid droplets containing internal, nucleoplasm-filled "bubbles." The complexity of these TDP43 phases suggests a remarkable ability of MLOs to form surface barriers and isolate components into internal vesicle-like structures, features that were previously thought to be unique to membrane-bound organelles.

RESULTS

TDP43 exists both in a soluble form and in irregular, nanometer-sized nuclear "speckles" in cells (Wang et al., 2002). In response to stress treatments, TDP43 assembles into spherical nuclear

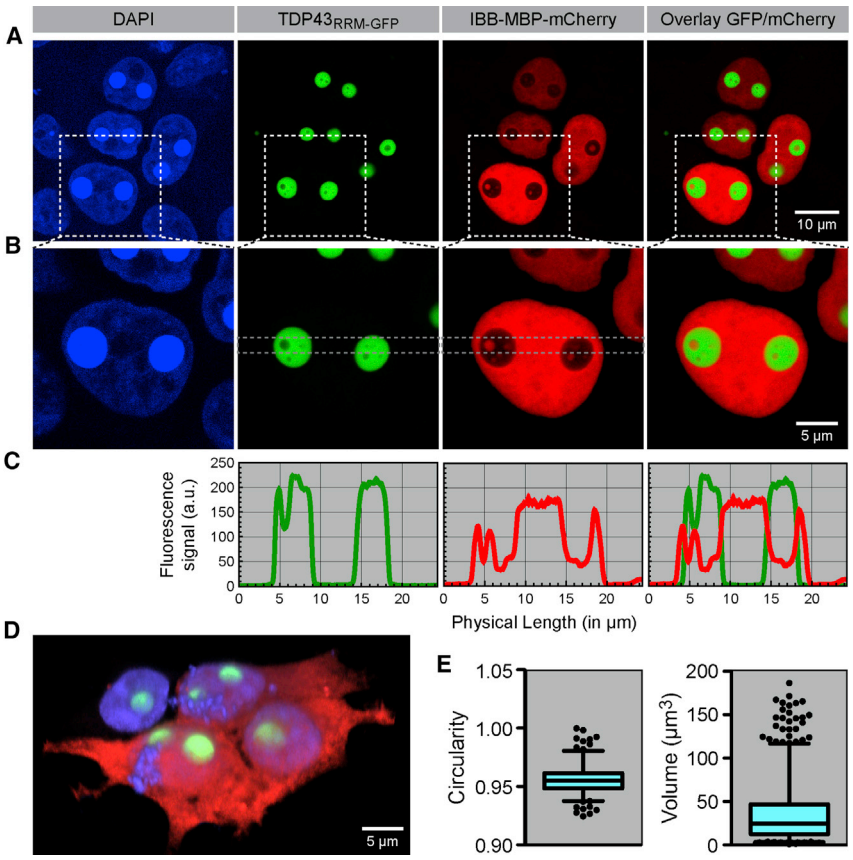

Figure 1. $TDP43_{RRM\text{-}GFP}$ Forms Micron-Sized Particles Containing Bubbles of Nucleoplasm

(A and B) $TDP43_{RRM\text{-}GFP}$ (green) and IBB-MBP-mCherry (red) were co-transfected into 293T cells. Boxed areas in (A) are shown magnified in (B). The GFP signal of the $TDP43_{RRM\text{-}GFP}$ particles was also detected in the blue channel, which corresponds to DAPI staining of DNA in nuclei.

(C) Stripe plots through the indicated region in B highlight that only the bubbles in the $TDP43_{RRM\text{-}GFP}$ particles contain IBB-MBP-mCherry.

(D) Reconstruction of 293T cells co-transfected with $TDP43_{RRM\text{-}GFP}$ and mCherry to illustrate relative dimensions.

(E) $TDP43_{RRM\text{-}GFP}$ particles, with a median circularity of 0.96, are highly spherical. The median particle radius is ~2 μm and the median volume ~25 μm^3. A total of 192 and 589 particles from three independent experiments were analyzed. Shown are box-whiskers-plots indicating median values (horizontal line) and 5%–95% percentiles (error bars); outliers are depicted as black points.

See also Figures S1–S4.

and cytoplasmic granules (Colombrita et al., 2009; Dewey et al., 2011; Udan-Johns et al., 2014). We speculated that a phase separation process drives this transformation. Indeed, analysis of stress-induced nuclear GFP-TDP43 foci by fluorescence recovery after photobleaching (FRAP) (Figures S1A–S1C) suggested that they behave similar to liquid assemblies formed by FUS (Patel et al., 2015). However, the small size of the stress-induced TDP43 granules made it difficult to study their dynamic properties in detail using imaging.

We also built versions of TDP43 in which four key phenylalanine residues were mutated (Buratti and Baralle, 2001) or the two central RRM domains were deleted, both to abolish RNA binding (Figure S1D). This approach was motivated by two considerations. First, the interaction between TDP43 and RNA is impaired under conditions of stress and is thought to initiate the formation of TDP43 assemblies in cells (Cohen et al., 2012, 2015). Second, the in vitro phase separation of full-length TDP43 (and related hnRNPs) did not require RNA, suggesting that the RRM domains are likely not essential for this process (Molliex et al., 2015). Inspired by a strategy recently used to demonstrate liquid-liquid phase separation of the germ granule component Ddx4 in vivo (Nott et al., 2015), we also generated a reporter in which we replaced the two RRM domains with GFP, hereafter referred to as $TDP43_{RRM\text{-}GFP}$. This internal GFP substitution allowed us to preserve the overall domain architecture of TDP43, rather than appending an additional folded domain to the predicted unstructured ends (Figures S2A and S2B).

$TDP43_{RRM\text{-}GFP}$ Forms Spherical Particles with Nucleoplasm-Filled Inclusions

When transfected into 293T cells, all TDP43 variants formed spherical assemblies independent of exposure to stress (Figure S1D). This phenotype was most pronounced for $TDP43_{RRM\text{-}GFP}$, which formed gigantic, spherical particles with a median radius of ~2 μm in the cell nuclei (Figure 1). Unexpectedly, the $TDP43_{RRM\text{-}GFP}$ particles contained internal inclusions filled with nucleoplasm, which could be readily seen when it was co-expressed with an ~75 kDa fusion protein composed of a nuclear localization signal, the *Escherichia coli* maltose binding protein and mCherry (IBB-MBP-mCherry). Particle formation was also seen when $TDP43_{RRM\text{-}GFP}$ was produced by stable expression and did not depend on the cell type, the identity of the fluorescent protein used to replace the RRM domains, or localization to the nucleus (Figure S3). These results suggested that TDP43 has an intrinsic potential to form elaborate sub-structured assemblies, independent of dedicated nucleic-acid binding domains or the nuclear environment. By nucleating the formation of giant structures, our $TDP43_{RRM\text{-}GFP}$ reporter provided an accessible in vivo model system for the visualization and analysis of internal substructures within MLOs.

Internal Inclusions Are Liquid "Bubbles" that Dynamically Rearrange within $TDP43_{RRM\text{-}GFP}$ Particles

Three-dimensional (3D) reconstitutions of confocal image stacks taken from live cells revealed that the internal inclusions were "bubbles" that move within the TDP43 particles on a timescale of minutes (Figure 2A), reminiscent of air bubbles moving through a viscous liquid such as honey or glycerol after agitation. Smaller bubbles fused into larger

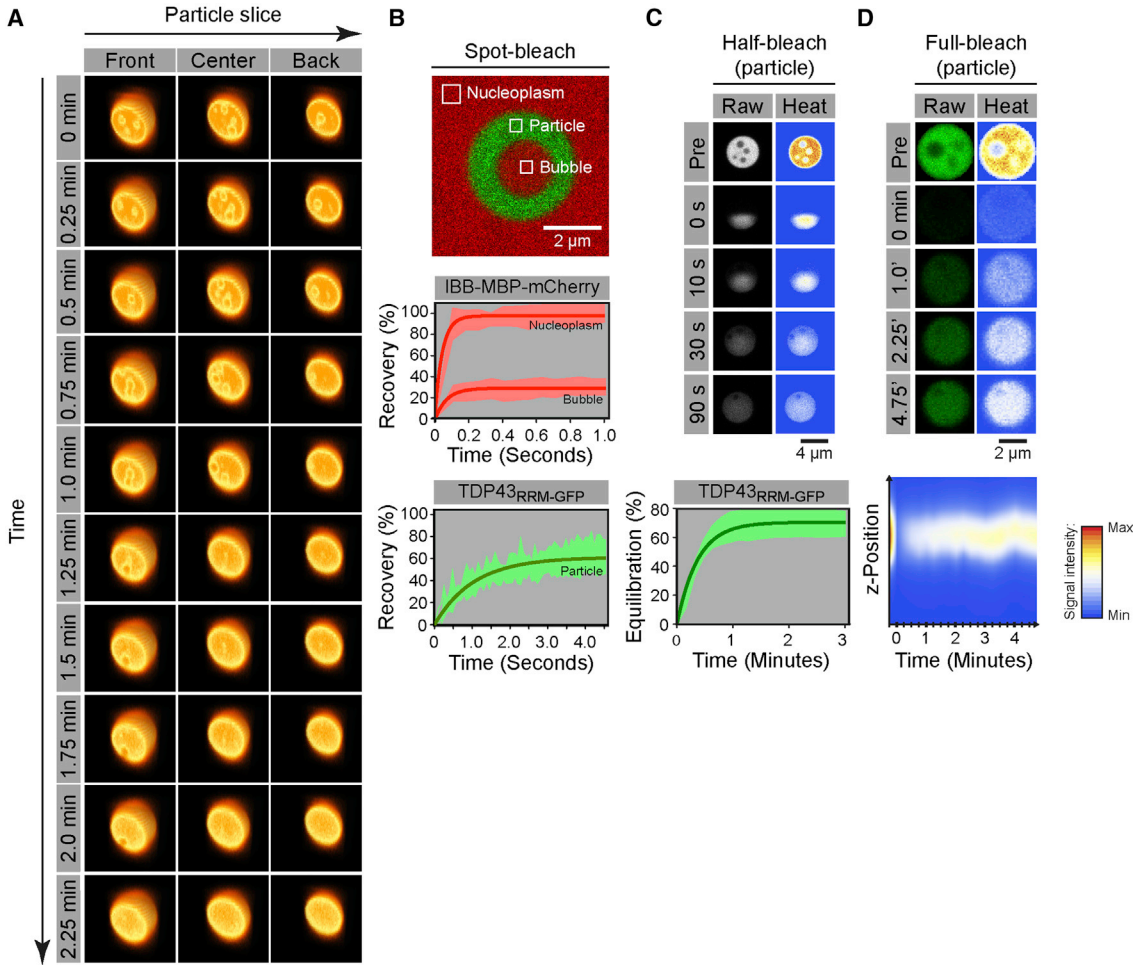

Figure 2. TDP43$_{RRM-GFP}$ Particles Are Multi-phase Liquid Droplets

(A) Time-resolved 3D image stacks reveal internal dynamics of TDP43$_{RRM-GFP}$ particles. Slices at three different levels through a reconstituted particle are shown over a time span of minutes. The rendering emphasized edges to highlight the boundaries of the particles and internal bubbles.

(B) Particles in which smaller bubbles had merged into a large, stable central bubble (top panel) were subjected to spot-bleach (small squares) and fluorescence recovery analysis to estimate the dynamics of IBB-MBP-mCherry in the nucleoplasm and bubbles (middle panel), as well as the dynamics of TDP43$_{RRM-GFP}$ in the particles (bottom panel). Plots show the time-dependent, normalized fluorescence recovery. Light red and green areas represent measurements (mean ± SD), and dark red and green lines show fits to one-phase exponentials.

(C) Half-bleach experiments were used to estimate the intra-particle dynamics of TDP43$_{RRM-GFP}$. The light green area represents measurements (mean ± SD), and the dark green line a one-phase exponential fit to the data.

(D) 4D FRAP experiments to analyze the partitioning of TDP43$_{RRM-GFP}$ monomers from the nucleoplasm into TDP43$_{RRM-GFP}$ particles. Fluorescence recovery over time is shown for a single central particle plane (upper panel) or by plotting the normalized average particle intensity of each recorded plane as a function of the z position (lower panel). At least six particles were analyzed for all experiments.

See also Figure S2 and Table S1.

ones, which were either excluded from the TDP43 particle or persisted as a single large central bubble. Interestingly, such dynamic bubbles have been known to exist in nucleoli for decades (see Discussion). We used FRAP to compare the mobility of IBB-MBP-mCherry in the nucleoplasm and within the bubbles of TDP43$_{RRM-GFP}$ particles (Figure 2B). In both regions, the recovery signal quickly reaches a plateau. However, the signal within the bubbles recovers to only ~20% of the initial value. This suggests that the bubbles are isolated from the bulk nucleoplasm, so that signal recovery solely results from monomer equilibration within the bubbles. Based on the FRAP experiments, we estimate the diffusion coefficient of IBB-MBP-mCherry in the nucleoplasm to be 5–15 $\mu m^2/s$, consistent with values reported in the literature (Moran et al., 2010). Our estimate for the diffusion coefficient of the same species in the bubbles of the TDP43 particles is 1–5 $\mu m^2/s$. Assuming that IBB-MBP-mCherry has a radius of ~4 nm, this suggests that the viscosities of the nucleoplasm (~7.5 mPa × s) and bubbles (~50 mPa × s) are in-between that of water (~1 mPa × sec) and most vegetable oils (<60 mPa × s), highlighting their liquid character.

$TDP43_{RRM\text{-}GFP}$ Particles Are Highly Viscous Liquid Droplets

Similar "spot-bleach" experiments revealed that the $TDP43_{RRM\text{-}GFP}$ molecules within the particles were also mobile (Figure 2B), consistent with a view of dynamic and rearranging interactions characteristic of a liquid (Hyman et al., 2014). However, in comparison to the nucleoplasm marker in the bubbles, $TDP43_{RRM\text{-}GFP}$ molecules in the particles require significantly longer (seconds instead of milliseconds) to recover fluorescence in a bleached area of identical size, leading to estimates for the diffusion coefficient of 0.1–0.5 $\mu m^2/s$ (Table S1). We also performed "half-bleach" FRAP experiments, which are commonly used to assess the internal mobility of protein phases (Brangwynne et al., 2009; Patel et al., 2015; Schmidt and Görlich, 2015). After bleaching one-half (of similarly sized) $TDP43_{RRM\text{-}GFP}$ particles, the fluorescence signal rapidly equilibrated between the two hemispheres, with a half-time ($t_{1/2}$) of ~15 s (Figure 2C). Considering the differences in length scales compared to the spot-bleach experiments, this amounts to a diffusion coefficient of 0.1–.5 $\mu m^2/s$ (Table S1). Assuming that a globular protein of average size would experience a similar diffusion coefficient and that the particles behave as Newtonian fluids, we approximate the viscosity of the particles in the order of ~1 Pa × s. This is ~1,000-times more viscous than water and similar to the viscosity of P granules, well-studied MLOs with liquid properties that are involved in the establishment of germ cell fate in worms (Brangwynne et al., 2009). Taken together, our data show that $TDP43_{RRM\text{-}GFP}$ can form micron-scale droplets composed of two apparently immiscible liquid phases with viscosities varying by almost one order of magnitude.

Dynamics of Exchange between $TDP43_{RRM\text{-}GFP}$ Particles and the Nucleoplasm

A key trait of MLOs is that they are in a dynamic equilibrium with their surroundings. To directly test for the exchange between the nucleoplasm and $TDP43_{RRM\text{-}GFP}$ particles, we performed "full-bleach" FRAP experiments where we bleached entire particles and followed the time-resolved fluorescence signal recovery in three-dimensional space (4D FRAP). We find that particle fluorescence recovered with a $t_{1/2}$ of ~1.5 min, suggesting that $TDP43_{RRM\text{-}GFP}$ monomers can indeed exchange between the particles and nucleoplasm (Figure 2D). However, even after 5 min, only ~40% of the initial fluorescence signal was recovered. We explain this based on the observation that the particles, in comparison to the nucleoplasm, are very bright and thus likely contain the majority of the $TDP43_{RRM\text{-}GFP}$ monomer pool in the cell, hence limiting the availability of fluorescent molecules for signal recovery after photobleaching. This prompted us to estimate the final concentration of $TDP43_{RRM\text{-}GFP}$ monomers in the particles. To correlate measured intensity signals with protein concentrations, we calibrated our setup with a titration series of purified recombinant GFP (Figure S4). We then quantified the fluorescence of $TDP43_{RRM\text{-}GFP}$ particles in live cells, yielding a final concentration of >1 mM or >50 mg/ml (Table S1). We also determined the fluorescence intensity in the vicinity of the $TDP43_{RRM\text{-}GFP}$ particles. This signal results from free monomers in solution and, assuming equilibrium conditions, reflects the critical concentration for phase separation, which we approximate to be ~5 μM (Table S1).

A Conserved Motif in the Intrinsically Disordered Region of TDP43 Regulates Phase Properties

In pathological contexts, disease-causing mutations increase the propensity of TDP43 to form irreversible aggregates (Johnson et al., 2009). This led us to consider the effects of sequence composition (Figure S2) on the properties of TDP43 droplets. ALS-associated mutations in TDP43 generally map to the C-terminal, NQ-rich low-complexity (LC) domain (Pesiridis et al., 2009). Interestingly, nearly half of them fall into a highly conserved and putatively structured 28 amino acid (aa) motif within this otherwise disordered and loosely conserved domain (Figures S2 and S5). This conserved region (CR; residues 320–348) is part of a longer stretch (321–366) that is thought to mediate interactions with other hnRNP family members and to be important for the splicing activity of TDP43 (D'Ambrogio et al., 2009). We either deleted the CR or replaced it with an equally long stretch of amino acids with the same composition as the rest of the LC domain (Figure S2; Supplemental Experimental Procedures). Under conditions where unperturbed $TDP43_{RRM\text{-}mCherry}$ formed bubble-containing particles, deletion of the CR greatly reduced the propensity for phase separation (Figure 3A). In contrast, replacement of the CR and consequent lengthening of the IDR led to the formation of an elaborate network of filaments nucleating from the remnants of a spherical core (Figures 3A and 3B). FRAP experiments did not reveal any significant fluorescence recovery even 20 min after bleaching, suggesting that these filamentous structures are stable aggregates (Figure 3C). Cells containing such aggregates showed significant growth defects compared to cells expressing mCherry alone or the unaltered WT $TDP43_{RRM\text{-}mCherry}$ protein (Figures 3D and 3E). We conclude that the CR within the prion-like IDR of TDP43 plays an important role in regulating both the formation and properties of TDP43 phases, either by direct sequence effects or indirectly by mediating protein interactions.

Formation of Composite Phases by Two Nearly Identical TDP43 Variants

Surprisingly, we found that co-expression of the aggregation-prone TDP43 variant together with wild-type (WT) $TDP43_{RRM\text{-}GFP}$ led to the formation of a composite phase in which bubble-containing, nearly spherical WT $TDP43_{RRM\text{-}GFP}$ "cores" were encapsulated by "mantles" comprised of both mutant $TDP43_{RRM\text{-}mCherry}$ and, to a smaller degree, WT $TDP43_{RRM\text{-}GFP}$ (Figures 3F and 3G). Half-bleach experiments revealed that the cores seem to be dynamic, showing intra-phase diffusion similar to the earlier described particles. In contrast, mutant $TDP43_{RRM\text{-}mCherry}$ in the mantles appeared to be immobile, consistent with a more solid structure (Figure 3G). The mantle phase, however, was not an impenetrable structure, as WT $TDP43_{RRM\text{-}GFP}$ molecules could partition into and move within it (Figure 3G). Co-expression of WT $TDP43_{RRM\text{-}GFP}$ thus substantially changed the morphology, and possibly the material properties, of the aggregates formed by mutant $TDP43_{RRM\text{-}mCherry}$.

Our results were unexpected given the supposedly promiscuous nature of the dynamic, low-affinity interactions between

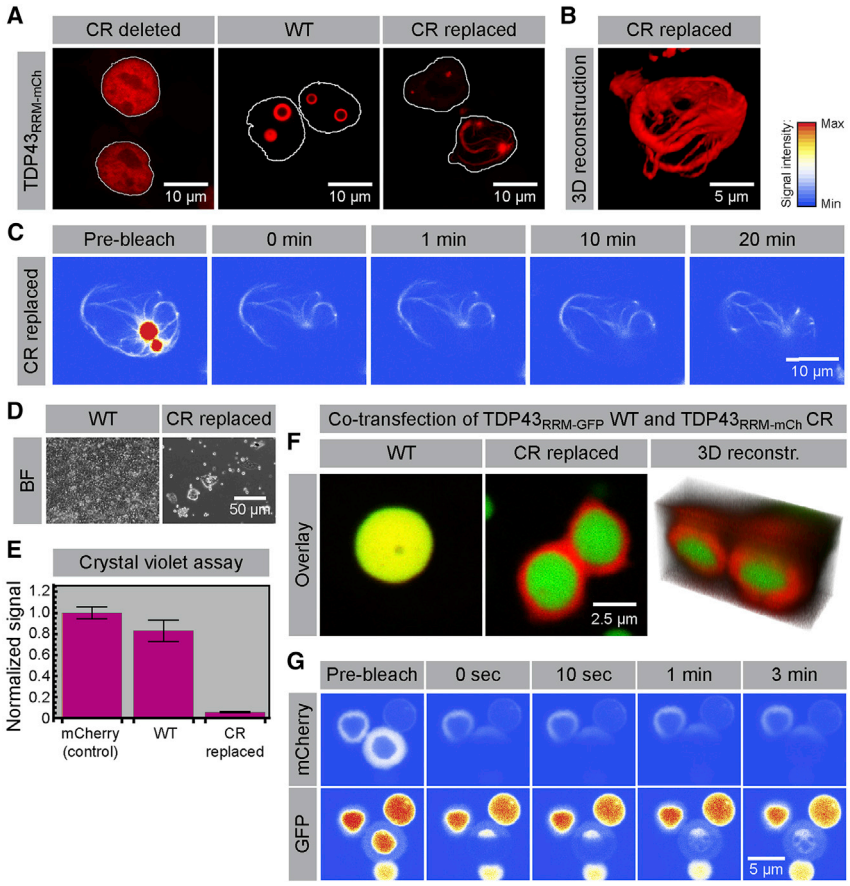

Figure 3. Formation of Toxic Fibrillar Aggregates and Multi-phase Composite Assemblies by TDP43 Sequence Variants

(A) Images of HEK293T cells transfected with either wild-type (WT) $TDP43_{RRM\text{-}mCherry}$ or $TDP43_{RRM\text{-}mCherry}$ variants in which the conserved region (CR) was deleted or replaced by a synthetic sequence designed to resemble the flanking IDR (see Figure S2 for details). Cell nuclei are outlined in white.

(B) 3D reconstructions of the filigree assemblies formed by the $TDP43_{RRM\text{-}mCherry}$ CR replacement variant.

(C) No fluorescence recovery is observed when the filamentous assemblies are bleached, suggesting that they represent stable aggregates or polymers.

(D) Bright-field (BF) images of $TPD43_{RRM\text{-}mCherry}$ droplet- and aggregate-containing cells 5 days after transfection.

(E) Assessment of cell death by crystal violet staining; shown are the crystal violet signals (normalized to the mCherry control) of three independent transfections for each construct (normalized mean ± SD).

(F) Co-expression of WT $TDP43_{RRM\text{-}GFP}$ (green) and the aggregation-prone $TDP43_{RRM\text{-}mCherry}$ CR variant (red) suppresses filament formation; instead a bipartite structure with a mantle around a central core is formed.

(G) FRAP analysis of the sub-structured bipartite TDP43 phases.

See also Figures S2 and S5.

IDRs, which has led to the hypothesis that related IDR-containing proteins are in constant danger of mislocalizing to the wrong MLOs or of conflating into a single common phase (Zhu and Brangwynne, 2015). Indeed, our observation that two phase separation-prone proteins with ~95% identical IDRs are immiscible and clearly separate into distinct, but closely opposed phases shows that small sequence differences can translate into dramatically altered physiochemical properties and demonstrates the significant complexity that can be generated by membrane-free structures.

Disease-Linked Single Amino Acid Changes Alter TDP43 Phase Properties

These striking results prompted us to study selected ALS/FTD-linked mutations that cause single amino acid changes within the IDR (abbreviated in standard single letter amino acid code hereafter). We focused on the M337V, N345K, and A382T mutations, because of their frequency in both familial and sporadic ALS, their known association with TDP43 pathology, and their presumptive impact on the secondary structure of the conserved motif within the IDR (Pesiridis et al., 2009) (Figure S2). Compared to WT $TDP43_{RRM\text{-}GFP}$ particles, all mutants also formed large, near-spherical particles in the nuclei of transfected cells and all demonstrated similar critical concentrations for phase separation (Figure 4A; Table S1). However, the M337V mutant formed much more homogenous condensates, containing a sharply reduced number of internal bubbles (Figure 4B). Half-bleach FRAP experiments showed that the intra-phase dynamics of the N345K and A382T mutant particles were comparable to those of WT particles (Figures 4C and 4D), leading to similar estimates for the diffusion coefficients and particle viscosities (Table S1). In contrast, M337V particles did not equilibrate after half-bleaching, indicating that the interactions between $TDP43_{M337V}$ monomers can no longer easily rearrange within the particles. Indeed, all reappearing fluorescence in half- or fully bleached particles resulted from the partitioning of unbleached monomers from the nucleoplasm into the outer particle shells (Figures 4C and 4D). We conclude that the liquid character of M337V particles is significantly reduced compared to WT particles, and this feature may explain the reduced propensity of these particles to contain bubbles (Figures 4B and 4D; Table S1). A382T and N345K particles had a different problem. 4D FRAP experiments revealed that the exchange of monomers between the particles and nucleoplasm was impaired, as hardly any fluorescence recovery was detected compared to WT particles (Figures 4E and 4F). Such partitioning defects can impact the phase behavior in many ways, including the ability to store and release molecules in the phase or to grow and shrink by monomer addition. Taken together, our findings show that single, disease-causing amino acid changes can have very specific and distinct effects on phase parameters. In MLOs, such alterations may influence function and perhaps even cause disease.

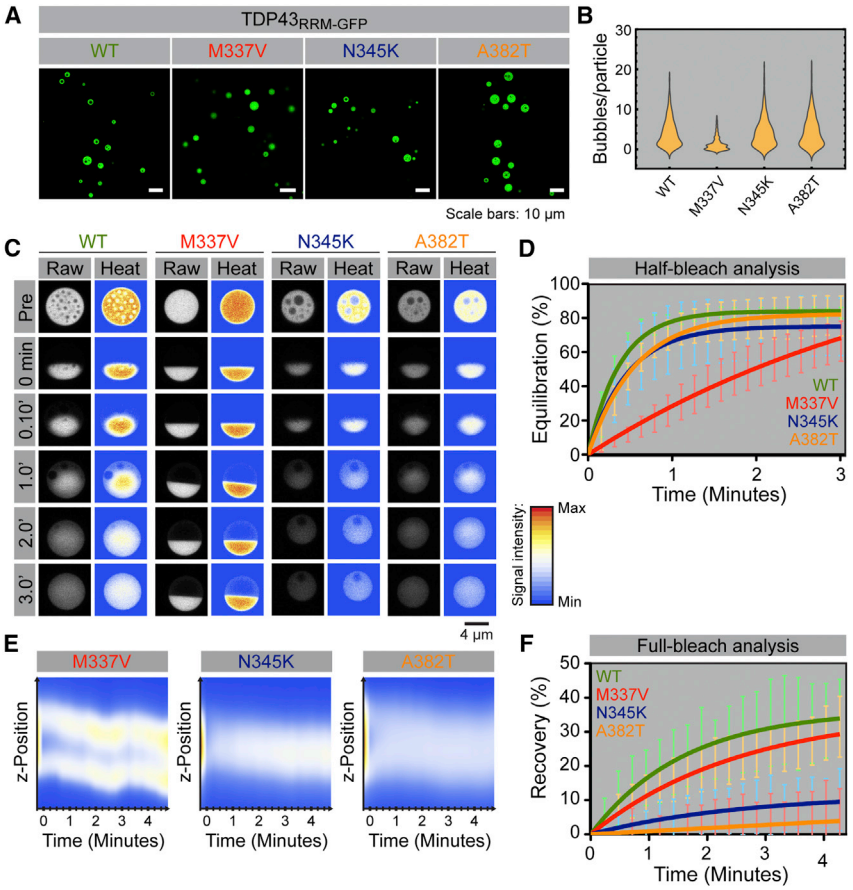

Figure 4. Impact of ALS/FTD-Linked Mutations on the Phase Properties of $TDP43_{RRM-GFP}$ Liquid Droplets

(A) Overview of HEK293T cells transfected with wild-type (WT) and mutant $TDP43_{RRM-GFP}$ reporters. Only the GFP channels are shown.

(B) Quantification of the number of bubbles per particle for WT (n = 423 particles analyzed; median number of bubbles per particle = 3), M337V (n = 570; median = 1), N345K (n = 466; median = 3), and A382T (n = 457; median = 4) particles.

(C) Half-bleach experiments of $TDP43_{RRM-GFP}$ droplets.

(D) FRAP analysis as in Figure 2C (see Table S1 for phase parameters). n ≥ 8 per construct. Shown are measurements (mean ± SD) and one-phase exponential curve fits.

(E) Full-bleach experiments as in Figure 2D.

(F) To compare multiple experiments (n ≥ 3 per construct), the normalized fluorescence recovery per particle was averaged over all recorded planes and plotted against time. Shown are measurements (mean ± SD) and one-phase exponential curve fits.

See also Figures S2, S4, and S5.

DISCUSSION

Liquid Bubbles in Membrane-less Organelles

Based on our observations that $TDP43_{RRM-GFP}$ particles contain internal bubbles of nucleoplasm, we speculate that MLOs comprised of TDP43 and/or other IDR-containing proteins may also contain similar liquid inclusions. Indeed, a series of recent studies established that nucleoli, prominent MLOs containing at least three morphologically different regions, are ensembles of coexisting liquid phases (Brangwynne et al., 2011; Weber and Brangwynne, 2015; Feric et al., 2016). Early investigations of nucleolar ultrastructure notably also generated a body of literature on "nucleolar vacuoles." These are spherical, protein-, and RNA-containing structures of varied size and number found in the nucleoli of both animal and plant cells (Johnson, 1969; Lewis, 1943). Almost 50 years ago, nucleolar vacuoles were already shown to be dynamic and capable of fusing with each other (Johnson and Jones, 1967), reminiscent of the bubbles in the $TDP43_{RRM-GFP}$ particles that we describe herein. These comparisons support the view that $TDP43_{RRM-GFP}$ particles represent a simplified mimic of sub-structured, multi-phase MLOs such as the nucleolus.

Possible Mechanisms of Bubble Formation

The finding that $TDP43_{RRM-GFP}$ phases contain liquid bubbles poses the question of how these structures form. In polymer chemistry, complex phase states with morphologies similar to the ones we observe for the nuclear $TDP43_{RRM-GFP}$ particles have been extensively studied in phase separated polymer blends (Cheng, 2008). If we consider a thermodynamic phase diagram for such a polymer blend (Figure S6), phase separation can occur either in the region defined by the spinodal curve or the metastable region between the spinodal and binodal curves. When the system is abruptly forced within the boundaries of the spinodal curve, phase separation instantaneously occurs by spontaneous (or spinodal) decomposition. In the metastable region, however, phase separation proceeds more slowly by nucleation-based growth, and phase morphologies are sensitive to perturbations. Indeed, such perturbations often can cause the formation of bubbles of one polymer embedded in droplets of the second (Cheng, 2008), reminiscent of the $TDP43_{RRM-GFP}$ particles we observe in cells.

Several considerations suggest that bubble-containing TDP43 phases likely form by nucleation-based phase separation under metastable conditions. First, spinodal decomposition usually occurs when a system is abruptly forced from the one-phase region into the two-phase region, for example by a sudden change in temperature or composition (Figure S6). However, such dramatic changes are unlikely to occur in our experiments, where cells were grown under controlled conditions. Second, the $TDP43_{RRM-GFP}$ concentration only gradually increases over time as a result of protein expression, at some point likely pushing the system into the metastable region (Figure S6). Finally, the "bubble-within-droplet" morphology we observe is characteristic of nucleation-based phase separation in the metastable region of the phase diagram. Spinodal decomposition, in contrast, typically results in a bicontinuous phase morphology,

which is not observed under the conditions of our experiments (Cheng, 2008).

The thermodynamically most stable state, however, would be a homogenous, bubble-free droplet. The fact that internal bubbles are readily observable, both in our $TDP43_{RRM-GFP}$ model system and MLOs such as nucleoli, indicates that these assemblies tend to be stuck in a local energy minimum or that cellular mechanisms to stabilize the bubble-containing state exist.

Multi-phase Assemblies as Membrane-less Mimics of Multi-vesicular Bodies

A morphological consequence of sub-compartmentalization within $TDP43_{RRM-GFP}$ droplets is that the interior of the bubbles and the parent environment, the nucleoplasm, are topologically related. This is reminiscent of multi-vesicular bodies (MVBs), specialized endosomes harboring internal membrane-bound vesicles, and suggests that MLOs may be able to sequester components from their parent environment into internal bubbles without the requirement that these components have to phase-separate themselves.

In the case of MVBs, a dedicated molecular machinery is required to select "cargoes" and bud-off vesicles (Piper and Katzmann, 2007). Specialized "diblock" proteins, comprised of a globular domain and a single N- or C-terminal IDR, may analogously bind to selected molecules and drive the formation of bubbles (Figure S7). The globular domain of such a protein-based surfactant could potentially interact specifically with the cargo in the bubble, while its IDR mediates overall solubility in the phase. In addition, a recent study suggested the intriguing possibility that specialized proteins could act as "cargo shuttles" between the parent environment and internal bubbles (Nott et al., 2016).

The composite phases formed by co-expression of TDP43 variants (Figures 3F and 3G), consisting of a solid mantle encapsulating a more liquid core, suggests a mechanism how such membrane-less MVB mimics can be further tuned. Apart from a possible role in stabilizing bubbles by preventing them from being excluded from the liquid core, the mantle phase may act as a selectively permeable barrier guarding the access to the core. The best-studied example for such an IDR-based "selective phase" is the permeability barrier of nuclear pore complexes, which controls macromolecular exchange between the nucleus and cytoplasm (Schmidt and Görlich, 2016).

Taken together, the similarities between membrane-less multi-phase assemblies and membrane-bound MVBs may extend beyond morphological resemblance. We suggest that multi-phase assemblies formed by IDR-containing proteins such as TDP43 may represent membrane-less analogs of MVBs. The differential solubility of certain molecules in the individual phases of composite assemblies may provide a simple and effective way to self-organize components and reactions in MLOs. Indeed, membrane-less multi-phase assemblies may have played important roles in evolution, allowing compartmentalization before the acquisition of endomembrane systems. This view is supported by a recent study suggesting that protoeukaryotes featured membrane-less nucleoli before they acquired membrane-bound organelles, including the nucleus, the endomembrane system, and mitochondria (Pittis and Gabaldón, 2016).

EXPERIMENTAL PROCEDURES

DNA Constructs and Cell Lines

All plasmids used in this study are summarized in Table S2. Sequences and maps are available upon request. TDP43 was obtained from Addgene (ID 27462). Bacterial and mammalian expression constructs were cloned into modified pQE80 (QIAGEN) and pCS-DEST backbones (Addgene 22423), respectively. For generation of stable, inducible T-REx-293 cell lines, the pcDNA5/FRT/TO backbone and the Flp-In system were used (Life Technologies).

Bacterial Protein Expression and Purification

GFP was expressed and purified using Ni(II) chelate chromatography under native conditions as previously described (Schmidt and Görlich, 2015).

In Vivo Phase Formation

Mammalian TDP43 expression constructs (500 ng) were transfected into HEK293T (obtained from ATCC), U2OS (gift of J. Lee, Stanford), or Neuro2A (a gift from B. Chaudhuri, Stanford) cells with X-tremeGENE 9 (Roche) and analyzed 24 hr later. Expression in stable cell lines was induced by addition of 1 μg/ml doxycycline for the indicated periods of time. Cells grown on poly-lysine coated glass coverslips were fixed with 4% paraformaldehyde (PFA) and mounted onto glass slides with Prolong Diamond mounting medium (Molecular Probes). For live cell imaging, cells were grown in poly-lysine coated μ-slides (ibidi). Prior to imaging, the culturing medium was exchanged to HEPES-buffered DMEM supplemented with 10% FBS (pH 7.4). Images were acquired on a Leica SP8 confocal laser scanning microscope equipped with a temperature- and gas-controlled incubation chamber (Life Imaging Services). Immersion objectives (Leica), 63× oil (NA 1.4) or 64× glycerol (NA 1.3), were used to image glass or plastic slides, respectively. The 405 nm, 488 nm, and 561 nm laser lines were used for excitation of DAPI (blue channel), GFP (green channel), or mCherry (red channel), respectively. Please see the Supplemental Experimental Procedures for details on image analysis.

Formation and Analysis of Composite TDP43 Phases

To form composite TDP43 phases, different combinations of $TDP43_{RRM-GFP}$ and $TDP43_{RRM-mCherry}$ constructs (375 ng each) were co-transfected into HEK293T cells. For FRAP analysis, particles were simultaneously bleached and imaged in both the GFP and mCherry channels.

Assessment of TDP43 Aggregate Toxicity

The indicated constructs were transfected into HEK293T cells and sorted 24 hr later by flow cytometry for mCherry-positive cells (on a Sony SH800 machine). The sorted cells were grown at 37°C and 5% CO_2 for 5 days and cell growth documented by acquiring bright-field images (using a Leica DM-IL microscope with a Leica DFC3000G camera) and staining with 0.5% (w/v) crystal violet in 25% methanol for 10 min at room temperature. After removing the dye, the dried plates were scanned using an Epson Perfection V700 digital scanner and the signal of each well quantified using Adobe Photoshop. All signals were normalized to the mCherry control transfection.

SUPPLEMENTAL INFORMATION

Supplemental Information includes Supplemental Experimental Procedures, seven figures, and two tables and can be found with this article online at http://dx.doi.org/10.1016/j.celrep.2016.06.088.

AUTHOR CONTRIBUTIONS

H.B.S. conducted and analyzed the experiments. H.B.S. and R.R. designed the study and wrote the paper.

ACKNOWLEDGMENTS

We thank the Deutsche Forschungsgemeinschaft (SCHM 3082/2-1 to H.B.S.) and the NIH/NIGMS (DP2 GM105448 to R.R.) for funding.

Received: March 29, 2016
Revised: June 2, 2016
Accepted: June 24, 2016
Published: July 21, 2016

REFERENCES

Alami, N.H., Smith, R.B., Carrasco, M.A., Williams, L.A., Winborn, C.S., Han, S.S., Kiskinis, E., Winborn, B., Freibaum, B.D., Kanagaraj, A., et al. (2014). Axonal transport of TDP-43 mRNA granules is impaired by ALS-causing mutations. Neuron *81*, 536–543.

Bergeron-Sandoval, L.P., Safaee, N., and Michnick, S.W. (2016). Mechanisms and consequences of macromolecular phase separation. Cell *165*, 1067–1079.

Brangwynne, C.P., Eckmann, C.R., Courson, D.S., Rybarska, A., Hoege, C., Gharakhani, J., Jülicher, F., and Hyman, A.A. (2009). Germline P granules are liquid droplets that localize by controlled dissolution/condensation. Science *324*, 1729–1732.

Brangwynne, C.P., Mitchison, T.J., and Hyman, A.A. (2011). Active liquid-like behavior of nucleoli determines their size and shape in Xenopus laevis oocytes. Proc. Natl. Acad. Sci. USA *108*, 4334–4339.

Buratti, E., and Baralle, F.E. (2001). Characterization and functional implications of the RNA binding properties of nuclear factor TDP-43, a novel splicing regulator of CFTR exon 9. J. Biol. Chem. *276*, 36337–36343.

Buratti, E., and Baralle, F.E. (2008). Multiple roles of TDP-43 in gene expression, splicing regulation, and human disease. Front. Biosci. *13*, 867–878.

Burke, K.A., Janke, A.M., Rhine, C.L., and Fawzi, N.L. (2015). Residue-by-Residue View of In Vitro FUS Granules that Bind the C-Terminal Domain of RNA Polymerase II. Mol. Cell *60*, 231–241.

Cheng, S.Z. (2008). Phase Transitions in Polymers: The Role of Metastable States (Amsterdam: Elsevier), pp. 77–155.

Cohen, T.J., Hwang, A.W., Unger, T., Trojanowski, J.Q., and Lee, V.M. (2012). Redox signalling directly regulates TDP-43 via cysteine oxidation and disulphide cross-linking. EMBO J. *31*, 1241–1252.

Cohen, T.J., Hwang, A.W., Restrepo, C.R., Yuan, C.X., Trojanowski, J.Q., and Lee, V.M. (2015). An acetylation switch controls TDP-43 function and aggregation propensity. Nat. Commun. *6*, 5845.

Colombrita, C., Zennaro, E., Fallini, C., Weber, M., Sommacal, A., Buratti, E., Silani, V., and Ratti, A. (2009). TDP-43 is recruited to stress granules in conditions of oxidative insult. J. Neurochem. *111*, 1051–1061.

D'Ambrogio, A., Buratti, E., Stuani, C., Guarnaccia, C., Romano, M., Ayala, Y.M., and Baralle, F.E. (2009). Functional mapping of the interaction between TDP-43 and hnRNP A2 in vivo. Nucleic Acids Res. *37*, 4116–4126.

Dewey, C.M., Cenik, B., Sephton, C.F., Dries, D.R., Mayer, P., 3rd, Good, S.K., Johnson, B.A., Herz, J., and Yu, G. (2011). TDP-43 is directed to stress granules by sorbitol, a novel physiological osmotic and oxidative stressor. Mol. Cell. Biol. *31*, 1098–1108.

Feric, M., Vaidya, N., Harmon, T.S., Mitrea, D.M., Zhu, L., Richardson, T.M., Kriwacki, R.W., Pappu, R.V., and Brangwynne, C.P. (2016). Coexisting liquid phases underlie nucleolar subcompartments. Cell *165*, 1686–1697.

Hyman, A.A., Weber, C.A., and Jülicher, F. (2014). Liquid-liquid phase separation in biology. Annu. Rev. Cell Dev. Biol. *30*, 39–58.

Johnson, J.M. (1969). A study of nucleolar vacuoles in cultured tobacco cells using radioautography, actinomycin D, and electron microscopy. J. Cell Biol. *43*, 197–206.

Johnson, J.M., and Jones, L.E. (1967). Behavior of nucleoli and contracting nucleolar vacuoles in tobacco cells growing in microculture. Am. J. Bot. *54*, 189–198.

Johnson, B.S., Snead, D., Lee, J.J., McCaffery, J.M., Shorter, J., and Gitler, A.D. (2009). TDP-43 is intrinsically aggregation-prone, and amyotrophic lateral sclerosis-linked mutations accelerate aggregation and increase toxicity. J. Biol. Chem. *284*, 20329–20339.

Kabashi, E., Valdmanis, P.N., Dion, P., Spiegelman, D., McConkey, B.J., Vande Velde, C., Bouchard, J.P., Lacomblez, L., Pochigaeva, K., Salachas, F., et al. (2008). TARDBP mutations in individuals with sporadic and familial amyotrophic lateral sclerosis. Nat. Genet. *40*, 572–574.

Lewis, W.H. (1943). Nucleolar vacuoles in living normal and malignant fibroblasts. Cancer Res. *3*, 531–536.

Li, Y.R., King, O.D., Shorter, J., and Gitler, A.D. (2013). Stress granules as crucibles of ALS pathogenesis. J. Cell Biol. *201*, 361–372.

Lin, Y., Protter, D.S., Rosen, M.K., and Parker, R. (2015). Formation and maturation of phase-separated liquid droplets by RNA-binding proteins. Mol. Cell *60*, 208–219.

Malinovska, L., Kroschwald, S., and Alberti, S. (2013). Protein disorder, prion propensities, and self-organizing macromolecular collectives. Biochim. Biophys. Acta *1834*, 918–931.

McDonald, K.K., Aulas, A., Destroismaisons, L., Pickles, S., Beleac, E., Camu, W., Rouleau, G.A., and Vande Velde, C. (2011). TAR DNA-binding protein 43 (TDP-43) regulates stress granule dynamics via differential regulation of G3BP and TIA-1. Hum. Mol. Genet. *20*, 1400–1410.

Mitrea, D.M., and Kriwacki, R.W. (2016). Phase separation in biology; functional organization of a higher order. Cell Commun. Signal. *14*, 1.

Molliex, A., Temirov, J., Lee, J., Coughlin, M., Kanagaraj, A.P., Kim, H.J., Mittag, T., and Taylor, J.P. (2015). Phase separation by low complexity domains promotes stress granule assembly and drives pathological fibrillization. Cell *163*, 123–133.

Moran, U., Phillips, R., and Milo, R. (2010). SnapShot: key numbers in biology. Cell *141*, 1262–1262.e1.

Nott, T.J., Petsalaki, E., Farber, P., Jervis, D., Fussner, E., Plochowietz, A., Craggs, T.D., Bazett-Jones, D.P., Pawson, T., Forman-Kay, J.D., and Baldwin, A.J. (2015). Phase transition of a disordered nuage protein generates environmentally responsive membraneless organelles. Mol. Cell *57*, 936–947.

Nott, T.J., Craggs, T.D., and Baldwin, A.J. (2016). Membraneless organelles can melt nucleic acid duplexes and act as biomolecular filters. Nat. Chem. *8*, 569–575.

Patel, A., Lee, H.O., Jawerth, L., Maharana, S., Jahnel, M., Hein, M.Y., Stoynov, S., Mahamid, J., Saha, S., Franzmann, T.M., et al. (2015). A liquid-to-solid phase transition of the ALS protein FUS Accelerated by disease mutation. Cell *162*, 1066–1077.

Pesiridis, G.S., Lee, V.M., and Trojanowski, J.Q. (2009). Mutations in TDP-43 link glycine-rich domain functions to amyotrophic lateral sclerosis. Hum. Mol. Genet. *18* (*R2*), R156–R162.

Piper, R.C., and Katzmann, D.J. (2007). Biogenesis and function of multivesicular bodies. Annu. Rev. Cell Dev. Biol. *23*, 519–547.

Pittis, A.A., and Gabaldón, T. (2016). Late acquisition of mitochondria by a host with chimaeric prokaryotic ancestry. Nature *531*, 101–104.

Schmidt, H.B., and Görlich, D. (2015). Nup98 FG domains from diverse species spontaneously phase-separate into particles with nuclear pore-like permselectivity. eLife *4*, e04251.

Schmidt, H.B., and Görlich, D. (2016). Transport selectivity of nuclear pores, phase separation, and membraneless organelles. Trends Biochem. Sci. *41*, 46–61.

Sreedharan, J., Blair, I.P., Tripathi, V.B., Hu, X., Vance, C., Rogelj, B., Ackerley, S., Durnall, J.C., Williams, K.L., Buratti, E., et al. (2008). TDP-43 mutations in familial and sporadic amyotrophic lateral sclerosis. Science *319*, 1668–1672.

Toretsky, J.A., and Wright, P.E. (2014). Assemblages: functional units formed by cellular phase separation. J. Cell Biol. *206*, 579–588.

Udan-Johns, M., Bengoechea, R., Bell, S., Shao, J., Diamond, M.I., True, H.L., Weihl, C.C., and Baloh, R.H. (2014). Prion-like nuclear aggregation of TDP-43 during heat shock is regulated by HSP40/70 chaperones. Hum. Mol. Genet. *23*, 157–170.

Wang, I.F., Reddy, N.M., and Shen, C.K. (2002). Higher order arrangement of the eukaryotic nuclear bodies. Proc. Natl. Acad. Sci. USA *99*, 13583–13588.

Wang, J.T., Smith, J., Chen, B.C., Schmidt, H., Rasoloson, D., Paix, A., Lambrus, B.G., Calidas, D., Betzig, E., and Seydoux, G. (2014). Regulation of RNA granule dynamics by phosphorylation of serine-rich, intrinsically disordered proteins in C. elegans. eLife *3*, e04591.

Weber, S.C., and Brangwynne, C.P. (2015). Inverse size scaling of the nucleolus by a concentration-dependent phase transition. Curr. Biol. *25*, 641–646.

Wippich, F., Bodenmiller, B., Trajkovska, M.G., Wanka, S., Aebersold, R., and Pelkmans, L. (2013). Dual specificity kinase DYRK3 couples stress granule condensation/dissolution to mTORC1 signaling. Cell *152*, 791–805.

Zhu, L., and Brangwynne, C.P. (2015). Nuclear bodies: the emerging biophysics of nucleoplasmic phases. Curr. Opin. Cell Biol. *34*, 23–30.